Energy-loss structure in core-level photoemission satellites of $SrTiO_3$, $SrTiO_3$:La, and $SrTiO_3$:Nb

Shigemi Kohiki
Department of Materials Science, Kyusyu Institute of Technology, Tobata, Kita-kyusyu 804-8550, Japan

Masao Arai, Hideki Yoshikawa, and Sei Fukushima
National Institute for Research in Inorganic Materials, Tsukuba, Ibaraki 305, Japan

Masaoki Oku
Institute for Materials Research, Tohoku University, Sendai 980-8577, Japan

Yoshio Waseda
The Institute for Advanced Materials, Tohoku University, Sendai 980-8577, Japan
(Received 14 January 2000; revised manuscript received 28 April 2000)

The core-level x-ray photoemission spectroscopy (XPS) satellites of single-crystalline $SrTiO_3$, $SrTiO_3$:La, and $SrTiO_3$:Nb *in situ* fractured in ultrahigh vacuum were compared with the electron-energy-loss spectrum and theoretical electron-energy-loss functions from first-principles electronic structure calculations. Experimental core-level XPS satellites of O 1*s* can be represented by peaks positioned at 6.1, 11.7, 14.2, 17.2, 19.7, 27.4, and 30.6 eV. The prominent features of theoretical electron-energy-loss functions agreed with those in the experimental satellites except the peaks around 20 eV.

I. INTRODUCTION

Aside from the technological importance of $SrTiO_3$, $SrTiO_3$:La, and $SrTiO_3$:Nb as a substrate for thin-film deposition of high-T_c superconductors and ferroelectrics because of their similar crystal structures and good lattice matching between them, the electronic structure of $SrTiO_3$ has been of fundamental interest since stoichiometric $SrTiO_3$ is highly insulating, but a slightly reduced compound shows superconductivity. Since $SrTiO_3$ crystallizes at room temperature (RT) in the simple-cubic perovskite structure ($a=3.9051$ Å),[1] it offers a natural starting point for the study of the electronic structure of many transition-metal oxides with similar crystal structure. The crystal-field splitting of the O $2p$ states occurs because the oxygen resides at a site of tetragonal D_{4h} $(4/mmm)$ point symmetry in $SrTiO_3$ with the simple cubic O_h^1 $(Pm3m)$ point symmetry. Many band calculations[2–4] and experimental works, including optical reflectance spectroscopy (ORS),[5,6] electron-energy-loss spectroscopy (EELS),[7–10] ultraviolet photoemission spectroscopy (UPS),[7,9,11–16] and x-ray photoemission spectroscopy (XPS),[17–21] have been performed for the electronic structure of $SrTiO_3$. The structure of the empty conduction band (CB) could play a decisive role as well as that of the valence band (VB) in the electronic properties of $SrTiO_3$ and related materials. In this paper we elucidate the experimental energy loss functions of $SrTiO_3$ using a first-principles computation of dielectric functions.

The XPS is suitable for examining the electronic structure of the filled levels and dielectric response of a solid. In addition to the chemical shifts of main peaks, we can extract the information about the electronic structure from the satellites generated by intrinsic and extrinsic processes. The intrinsic satellites are caused by several mechanisms under the influence of a core hole. For example, it is well known that the charge-transfer (CT) relaxation[22,23] in the photoemission final states dominates the core XPS satellites of late transition-metal compounds since the Coulomb interaction energy between the Cu $2p$ core hole and Cu $3d$ electrons is larger than the VB width. Thus, the $2p$ core-hole potential largely lowers the energy of the $3d$ levels, then ligand electrons transfer to the Cu $3d$ states in order to screen the core-hole charge. It was also argued that the CT mechanism may describes the XPS satellites of early transition-metal compounds.[19,24–26] The exciton mechanism was also proposed as the origin of intrinsic satellites.[27]

The extrinsic satellites are caused by the dielectric response of valence electrons to the photoexcited electrons. During the approach of an excited electron to the solid surface, the Coulomb field accompanied with the moving electron interacts with the electrons in the solid via long-range dipole fields. The long-range Coulomb interactions bring about interband transitions and plasma excitations. These excitations cause the electron-energy-loss structure on the lower kinetic energy side of core lines. High-resolution XPS can reveal the characteristic energy loss structure and thus can probe unoccupied electronic states of insulators.[28] To investigate intrinsic satellites quantitatively, it is necessary to determine extrinsic satellites since observed satellites are the convolution of intrinsic and extrinsic structures. Though the physical explanation of the extrinsic satellites is simple, they have not been extensively compared with the theoretical results. The purpose of present paper is to analyze the extrinsic satellites of $SrTiO_3$ by comparing with experimental EELS spectrum and theoretical energy-loss functions. In Sec. II, we show the observed XPS core spectra. The satellite structures are compared with theoretical electron-energy-loss functions and the experimental EELS spectrum in Sec. III.

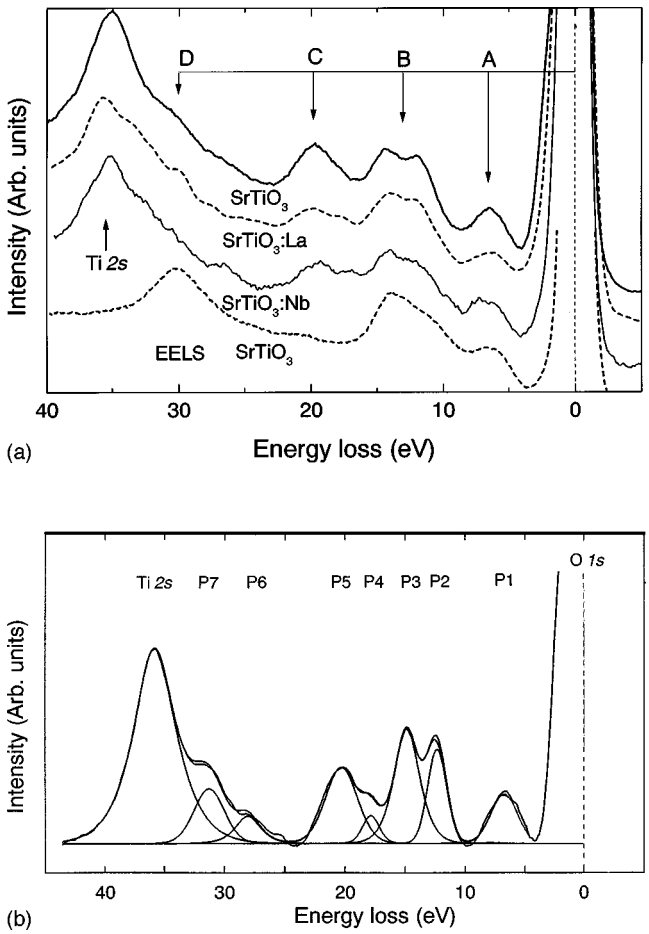

FIG. 1. (a) Experimental photoemission spectra for the O 1*s* electrons of $SrTiO_3$, $SrTiO_3$:La, and $SrTiO_3$:Nb *in situ* fractured in UHV. Electron-energy-loss spectrum with a primary-electron energy of 1000 eV is also shown for comparison. (b) Curve fitting for the O 1*s* spectrum of $SrTiO_3$.

II. EXPERIMENTAL RESULTS

The XPS measurements were performed by using the single-crystal samples fractured *in situ* in ultrahigh vacuum (UHV) since it is the only reliable way to prepare almost perfect and stoichiometric surfaces indispensable for studying intrinsic surface properties of oxides. The gross electronic structure of the fractured surfaces reflects that of perfect surfaces. For XPS measurements at RT we used a Surface Science Laboratories Model SSX-100 spectrometer with a monochromatized Al $K\alpha$ source having a spot diameter of 300 μm on the sample surface. The pass energy of the spectrometer was set to 50 eV. The solid angle of the input lens of the energy analyzer was 30°. The spectrometer was calibrated utilizing the Au $4f_{7/2}$ electrons (83.79 eV) and the full width at half maximum (FWHM) of the Au $4f_{7/2}$ peak was 1.03 eV.

As pointed out by Egdell and Naylor,[9] no EELS or UPS spectra could be observed without any reduction of the insulator such as $SrTiO_3$. In this experiment we used $SrTiO_3$ (001) single crystals of undoped (intrinsic) and doped with 3 at.% La and with 1 at.% Nb (*n* type). Both *n*-type $SrTiO_3$ crystals are highly conductive and no charge shift was observed. For the undoped $SrTiO_3$, the charge shift was corrected with the Ti $2p_{3/2}$ electrons as 459.2 eV, which is the

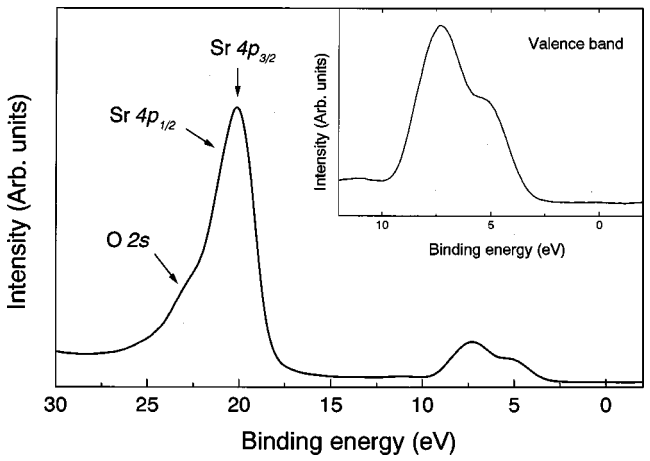

FIG. 2. Valence band (VB) spectrum of $SrTiO_3$ including the Sr 4*p* and O 2*s* levels. The Fermi energy was determined by setting the Ti $2p_{3/2}$ electron binding energy to 459.2 eV.

value obtained for doped *n*-type $SrTiO_3$ crystals. The spectra for the undoped sample were taken with an electron flood of about 1 eV. The samples were fractured in a vacuum of 4×10^{-10} Torr at the analyzing position of the analyzer chamber, and then we immediately started the measurement of as-fractured spectra. No contamination signals could be detected for 20 min after the fracturing.

Core electrons in the orbitals shallower than Ti 2*s* can be excited by Al $K\alpha$ radiation. The core lines are followed by satellite structure ranging from 5 to 30 eV relative to the zero-loss line. The most intense and best resolved line is the O 1*s* as shown in Fig. 1(a). Within the experimental uncertainty the satellite structure is identical for *in situ* fractured $SrTiO_3$, $SrTiO_3$:La, and $SrTiO_3$:Nb. The observed features in the satellites agree with the previous experiments.[20]

As shown in Fig. 1(b), the observed O 1*s* satellites can be represented by seven components positioned at 6.1, 11.7, 14.2, 17.2, 19.7, 27.4, and 30.6 eV. Mayer *et al.*[20] fitted the O 1*s* XPS satellites below 35 eV with eight components. Without any considerations of surface and bulk electron-energy-loss functions, they assigned two components as plasmon excitation and the other five as interband transition. Our first-principles calculation does not support such an assignment, as shown in next section.

Reduced local coordination of surface ions decreases the Madelung potential energies at the surface from the bulk values and causes the surface electronic levels in the bulk band gap (E_g). Figure 2 shows the VB spectrum of *in situ* fractured $SrTiO_3$. The VB spectra of *in situ* fractured $SrTiO_3$, $SrTiO_3$:La, and $SrTiO_3$:Nb are similar to each other. The VB spectra exhibited two peaks around 5 and 7 eV arising from the O $2p$ π and σ bonding orbitals, respectively. The features in the VB of as-fractured samples are in agreement with those reported by UPS (Refs. 7, 9, 12–16) and XPS (Refs. 17–19 and 21). The experimental width of the VB, determined from the both intercepts of linear fits to the left shoulder of the 5 eV peak and the right shoulder of the 7 eV peak with the zero line, of the samples was 6 eV, which agrees with those reported by UPS (Refs. 7, 15, and 16) and XPS (Ref. 17).

The valence-band maximum (VBM), determined from the intercept of a linear fit to the left shoulder of the 5 eV peak

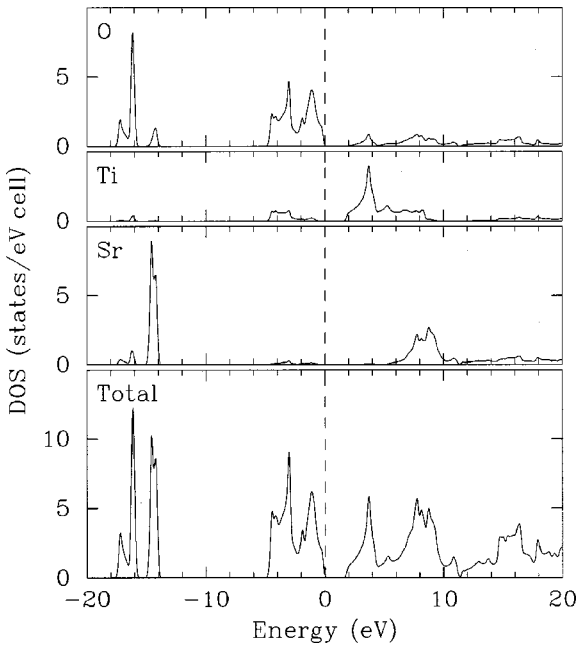

FIG. 3. Calculated total density of states (DOS) and partial densities of states (PDOS) of each atom.

with the zero line, of the samples lies at 3.3 eV below the Fermi level (E_F). This VBM position in XPS agrees well those reported by UPS (Refs. 7 and 13–15) within the experimental uncertainty (± 0.1 eV). Since the reported optical E_g is 3.27 eV,[29,30] the bulk E_F is positioned at the bottom of the conduction band within the experimental uncertainty (± 0.1 eV), which suggests that the band bending is negligibly small for *in situ* fractured surfaces. No prominent emission from the region of bulk E_g was observed in this XPS experiment. There are no clear intrinsic surface states in the region of the bulk E_g for *in situ* fractured $SrTiO_3$, $SrTiO_3$:La, and $SrTiO_3$:Nb. Alteration to the electron energy loss function is scarcely expected from the empty surface states.

III. THEORETICAL RESULTS AND DISCUSSION

We calculated the bulk electronic structures of $SrTiO_3$ within the local density approximation,[31] using the WIEN97 package[32] which is based on the full-potential linear augmented-plane-wave method. The resulting total and partial density of states (DOS) are shown in Figs. 3 and 4. The calculated DOS of valence bands agrees fairly well with the experimental VB spectrum shown in Fig. 2. The valence bands are mainly composed of the O $2p$ orbital. The Ti $3d$ orbital also contributes to the valence bands by the p-d hybridization. Below the valence bands, O $2s$ and Sr $4p$ orbitals form narrow semicore bands. The states at the bottom of the empty conduction bands arise from the threefold degenerate Ti $3d$ t_{2g} orbital, which has lower energy than the twofold degenerate Ti $3de_g$ orbital. The Ti $3de_g$ orbital hybridizes with the Sr $5s$ and $4d$ orbitals and is distributed in a wider energy region than the t_{2g} orbital.

The theoretical electron-energy-loss functions $-\mathrm{Im}[\epsilon^{-1}]$ were obtained from the wave functions and energy bands. The imaginary part of dielectric functions ϵ was

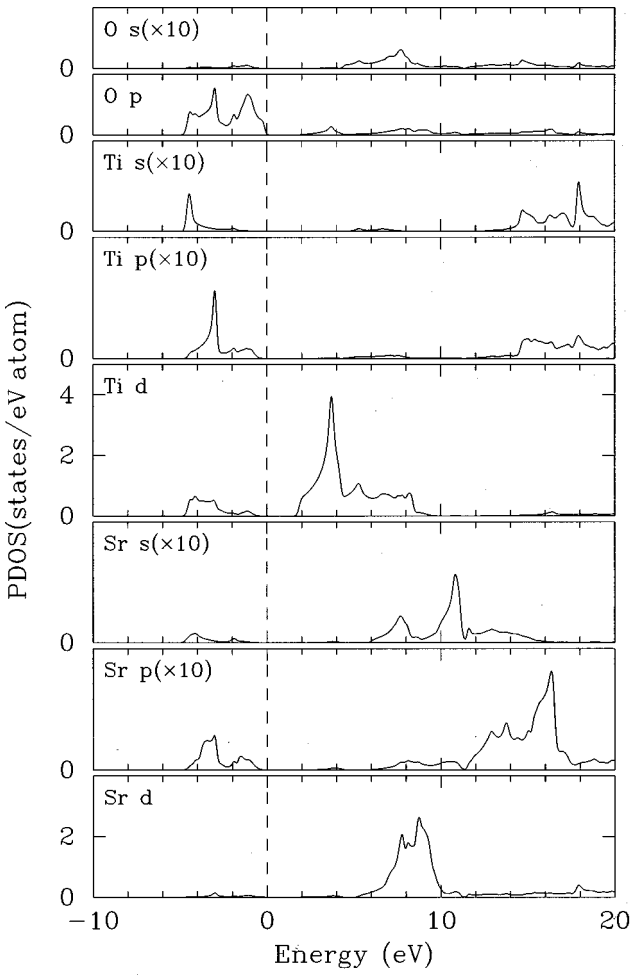

FIG. 4. Calculated partial densities of states (PDOS) projected by angular momentum around each atom. The PDOS labeled by $(\times 10)$ are magnified 10 times.

calculated from the momentum matrix elements between the occupied and unoccupied wave functions.[33] The real part $\mathrm{Re}[\epsilon]$ was evaluated from the $\mathrm{Im}[\epsilon]$ by the Kramers-Kronig transformation. The electron-energy-loss functions of bulk $-\mathrm{Im}[\epsilon^{-1}]$ and surface[34] $-\mathrm{Im}[(\epsilon+1)^{-1}]$ were derived from the calculated dielectric functions. The $\mathrm{Im}[\epsilon]$ and $\mathrm{Re}[\epsilon]$ of the dielectric function and the $-\mathrm{Im}[\epsilon^{-1}]$ and $-\mathrm{Im}[(\epsilon+1)^{-1}]$ are shown in Fig. 5. The peaks in the $-\mathrm{Im}[(\epsilon+1)^{-1}]$ tend to shift to the lower-energy side than in the $-\mathrm{Im}[\epsilon^{-1}]$.

The $\mathrm{Im}[\epsilon]$ shows various structures caused by the interband transition. The transition between O $2p$ valence bands and Ti $3d$ conduction bands contribute to prominent features between 2 and 12 eV. The broad peaks between 18 and 25 eV are from the transition between semicore states (Sr $4p$ and O $2p$) and conduction bands. Other small features arise from the transition between valence bands and higher conduction bands.

Corresponding to the various features in the $\mathrm{Im}[\epsilon]$, the energy-loss function also shows three prominent features (I, II, and III) as shown in Fig. 5. Feature III at 28 eV is most dominant and can be assigned as a plasmonlike collective excitation of the valence and semicore electrons since the energy fairly agrees with the plasmon energy 26.4 eV predicted naively from the electron density (0.504

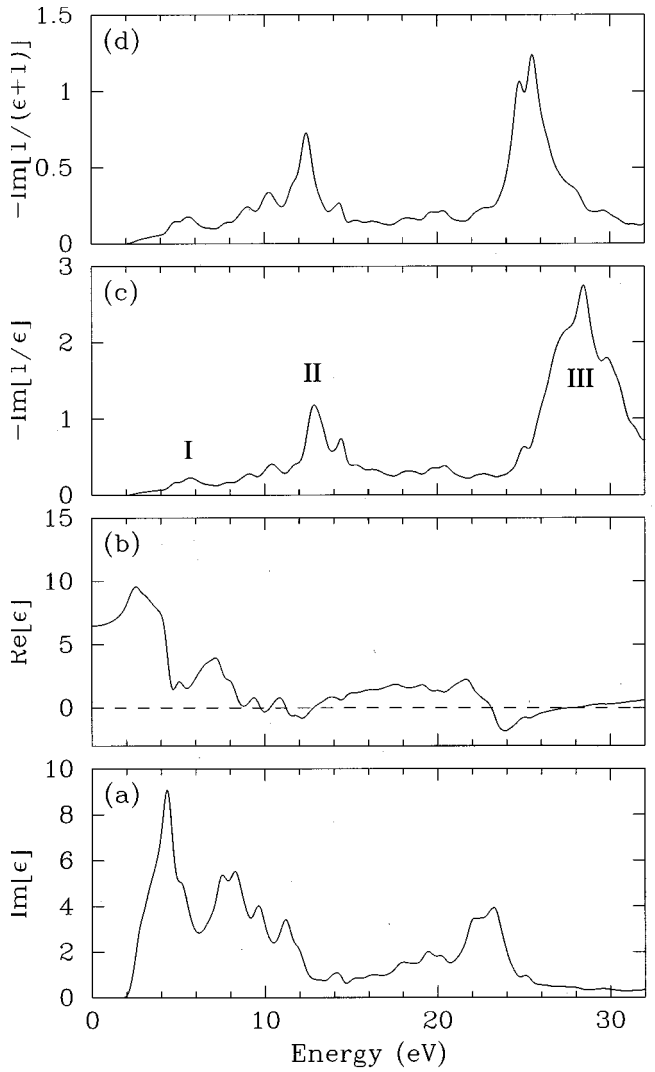

FIG. 5. Calculated dielectric function and electron-energy-loss functions of $SrTiO_3$. (a) Imaginary part and (b) real part of the theoretical dielectric function, (c) bulk and (d) surface theoretical electron-energy-loss functions.

electrons/Å^3). Feature II around 13 eV arises from the resonance of the O $2p$ valence electron. The plasmon excitation energy from the O $2p$ valence electron density (0.303 electron/Å^3) are estimated as 20.4 eV. Therefore, it is largely shifted by the influence of other interband transitions. The small feature I around 5 eV is caused by the splitting of the Ti $3d$ conduction bands into t_{2g} and e_g subbands.

The prominent structures in the theoretical electron-energy-loss functions [I, II, and III in Fig. 5(c)] are similar to those in the satellites [A, B, and D in Fig. 1(a)]. Feature III is positioned at a slightly lower-energy region than the experimental feature D. Theoretically, feature III around 28 eV is due to the influence of the interband transitions between semicore Sr $4p$ and O $2s$ levels and conduction bands. The disagreement with the XPS measurements may be caused by the underestimation of the energy level of semicore states. Namely, it arises from the incorrect position of the Sr $4p$ and O $2s$ levels in the calculations since the local-density approximation underestimates the binding energies of the localized states. From the comparison with the experimental Sr

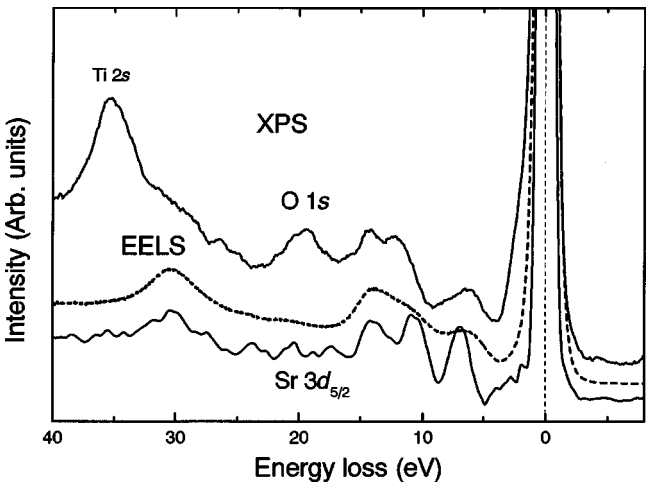

FIG. 6. Sr $3d_{5/2}$ spectrum, which is generated from that of the observed Sr $3d$ by the spin-orbit stripping procedure. O $1s$ and EELS spectra are also shown for comparison.

$4p$ and O $2s$ binding energy, the calculated Sr $4p$ and O $2s$ states should appear at 2 eV lower-energy region relative to the conduction-band minimum (CBM) where the Fermi level is pinned in the experiment. If we shift the theoretical Sr $4p$ and O $2s$ levels to the experimental positions, theoretical feature III would move to the experimental energy range.

In the theoretical electron-energy-loss functions, there is no clear-cut structure around 20 eV where the XPS satellites show the broad peak C. To clarify the discrepancy, the EELS spectra of *in situ* fractured $SrTiO_3$ were measured by using a PHI Model 500 spectrometer with a LaB_6 electron gun in a pressure less than 5×10^{-10} Torr. The incident kinetic energy was set to 1000 eV so that it corresponds to the kinetic energy of the photoexcited electrons from O $1s$ (950 eV) and Ti $2p$ (1020 eV). The spectrum is shown in Fig. 1(a). It is obvious that the energy-loss structures by EELS agree with O $1s$ XPS satellites except the peaks around 20 eV. The spectral intensity around 20 eV in EELS is smaller than that in XPS and is consistent with that expected from the theoretical calculation. Thus, the peak C cannot be assigned as an energy-loss structure. It may be interpreted as a loss structure by surface plasmons since the peak position is almost at 28 eV/$\sqrt{2}\approx$20 eV. However, the simple relation for plasma frequencies of bulk ω_p and surface ω_s,

$$\omega_s = \omega_p/\sqrt{2}, \tag{1}$$

is not always satisfied for materials with complex electronic structures. If the relation is satisfied for the present system, we would see a peak at 20 eV in calculated $-\mathrm{Im}[(\epsilon+1)^{-1}]$. The absence of such a peak in Fig. 5(d) excludes the possibility of surface plasmons. At present, the origin of the peak has not yet become clear. It may be caused by the excitation of valence or semicore states during the photoexcitation of core electrons (shake-up or shake-off process).

The Sr $3d$ and Ti $2p$ satellites have a structure similar to the O $1s$ satellite. To show it clearly, the Sr $3d$ satellites are decomposed to $3d_{5/2}$ and $3d_{3/2}$ components by a spin-orbit stripping procedure. The $3d_{5/2}$ spectrum is shown in Fig. 6. The peak positions of O $1s$ and Sr $3d_{5/2}$ satellites agree well except for the peak at 20 eV. Since this peak is not caused by

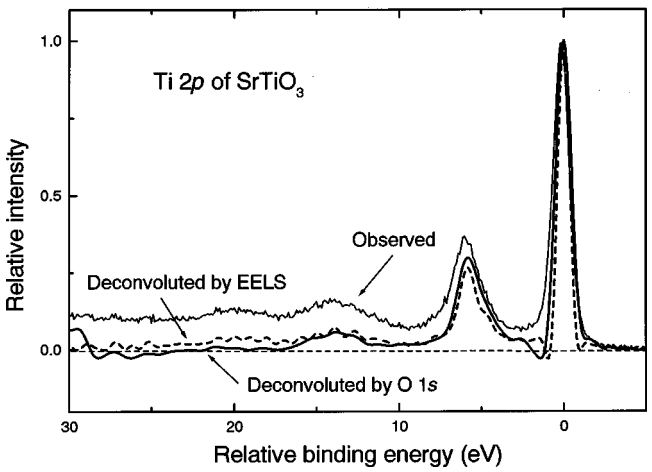

FIG. 7. Thin line shows observed Ti $2p$ spectrum. The intrinsic part of the Ti $2p$ spectrum is generated by removing the contribution of extrinsic process. Solid and dashed lines are the results using O $1s$ and EELS spectrum as a response function, respectively.

the energy-loss process as explained in the previous paragraph, it is natural that Sr $3d_{5/2}$ does not have a peak at 20 eV.

The Ti $2p$ satellites cannot be decomposed into $2p_{3/2}$ and $2p_{1/2}$ since the broadening of two main lines are different. We analyzed the contribution of the energy-loss process by subtracting it from the Ti $2p$ satellites as previously reported in Ref. 35. Figure 7 shows the Ti $2p$ spectra obtained by deconvolution of observed spectrum using O $1s$ or EELS spectra as a response function. The figure shows that the satellites with high binding energy are affected by the electron-energy-loss functions. When the O $1s$ spectrum is used as a response function, no intrinsic satellites remain at binding energies higher than 15 eV. The residual structure may be caused by the intrinsic mechanisms such as CT or excitons and their quantitative analysis must be performed after subtraction of the background due to the energy-loss process.

IV. CONCLUSION

We have presented experimental XPS spectra of $SrTiO_3$, $SrTiO_3$:La, and $SrTiO_3$:Nb. No intrinsic surface states exist in the bulk band gap for *in situ* fractured samples. The theoretical energy-loss functions are in good agreement with the O $1s$ and Sr $3d$ XPS satellites. It indicates that most of these satellite structures are due to the energy-loss process of photoexcited electrons. The exception is the peak around 20 eV, which only appears in the O $1s$ spectrum. Even for Ti $2p$ satellites, the effect of the energy-loss process is not negligible.

ACKNOWLEDGMENTS

The authors thank T. Maruyama for his assistance in a part of XPS, P. Blaha, K. Schwarz, and J. Luiz for providing us their WIEN97 programs, and T. Sato of the Institute for Advanced Materials, Tohoku University, for EELS. A part of this work was performed at the Laboratory for Developmental Research of Advanced Materials, the Institute for Materials Research, Tohoku University.

[1] R. W. G. Wyckoff, *Crystal Structures II* (Interscience, New York, 1964).
[2] A. H. Kahn and A. J. Leyendecker, Phys. Rev. **135**, A1321 (1964).
[3] L. F. Mattheis, Phys. Rev. B **6**, 4718 (1972).
[4] F. M. F. de Groot, J. Faber, J. J. M. Michiels, M. T. Czyzyk, M. Abbate, and J. C. Fuggle, Phys. Rev. B **48**, 2074 (1993).
[5] M. Cardona, Phys. Rev. **140**, A651 (1965).
[6] A. M. Mamedov, Ferroelectrics **45**, 55 (1982).
[7] V. E. Henrich, G. Dresselhaus, and H. J. Zeiger, Phys. Rev. B **17**, 4908 (1978).
[8] V. M. Vermudez and V. H. Ritz, Chem. Phys. Lett. **73**, 160 (1980).
[9] R. G. Egdell and P. D. Naylor, Chem. Phys. Lett. **91**, 200 (1982).
[10] A. Hirata, K. Saiki, A. Koma, and A. Ando, Surf. Sci. **319**, 267 (1994).
[11] R. A. Powell and W. E. Spicer, Phys. Rev. B **13**, 2601 (1976).
[12] W. J. Lo and G. A. Somorjai, Phys. Rev. B **B17**, 4942 (1978).
[13] Y. W. Chung and W. B. Weissbard, Phys. Rev. B **20**, 3456 (1979).
[14] R. Courths, Phys. Status Solidi B **100**, 135 (1980).
[15] V. E. Henrich and R. L. Kurtz, J. Vac. Sci. Technol. **18**, 416 (1981).
[16] B. Reihl, J. G. Bednorz, K. A. Muller, Y. Jugnet, G. Landgren, and J. F. Morar, Phys. Rev. B **30**, 803 (1984).
[17] F. L. Battye, H. Hochst, and A. Goldmann, Solid State Commun. **19**, 269 (1976).
[18] S. P. Kowalzyk, F. R. McFeely, L. Ley, V. T. Gritsyna, and D. A. Shirley, Solid State Commun. **23**, 161 (1977).
[19] A. E. Bocquet, T. Mizokawa, K. Morikawa, A. Fujimori, S. R. Barman, K. Maiti, D. D. Sarma, Y. Tokura, and M. Onoda, Phys. Rev. B **53**, 1161 (1996).
[20] B. Mayer, S. Maehl, and M. Neumann, Z. Phys. B **101**, 85 (1996).
[21] Y. Adachi, S. Kohiki, K. Wagatsuma, and M. Oku, J. Appl. Phys. **84**, 2123 (1998).
[22] S. Larsson, Chem. Phys. Lett. **40**, 362 (1976).
[23] G. van der Laan, C. Westra, C. Haas, and G. A. Sawatzky, Phys. Rev. B **23**, 4369 (1981).
[24] S. Larsson, J. Electron Spectrosc. Relat. Phenom. **8**, 171 (1976).
[25] K. Okada, T. Uozumi, and A. Kotani, J. Phys. Soc. Jpn. **63**, 3176 (1994).
[26] J. C. Parlebas, Phys. Status Solidi B **178**, 9 (1993).
[27] D. K. G. de Boer, C. Haas, and G. A. Sawatzky, Phys. Rev. B **29**, 4401 (1984).
[28] S. Kohiki, M. Arai, H. Yoshikawa, and S. Fukushima, Phys. Rev. B **57**, 14 572 (1998).
[29] M. Capzzi and A. Frova, Phys. Rev. Lett. **25**, 1298 (1970).
[30] C. Lee, J. Destry, and J. L. Brebner, Phys. Rev. B **11**, 2299 (1975).
[31] For a review, R. O. Jones and O. Gunnarsson, Rev. Mod. Phys. **61**, 689 (1989).
[32] P. Blaha, K. Schwarz, and J. Luitz, WIEN97, Vienna University of Technology 1997. [Improved and updated UNIX version of the

original copyrighted WIEN code, which was published by P. Blaha, K. Schwarz, P. Sorantin, and S. B. Tricky, Comput. Phys. Commun. **59**, 399 (1990).]

[33] R. Abt, C. Ambrosch-Draxl, and P. Knoll, Physica B **194-196**, 1451 (1994).

[34] D. L. Mills, Surf. Sci. **48**, 59 (1975).

[35] M. Oku, K. Wagatsuma, and S. Kohiki, Phys. Chem. Chem. Phys. **1**, 5327 (1999).